Cellular Oncology 27 (2005) 183–190
IOS Press

Quantitative analysis of chemotherapeutic effects in tumors using *in vivo* staining and correlative histology

Heung Kook Choi [a,b,*], Doreen Yessayan [a], Hyun Ju Choi [b], Eyk Schellenberger [a], Alex Bogdanov [a], Lee Josephson [a], Ralph Weissleder [a] and Vasilis Ntziachristos [a]

[a] *Center for Molecular Imaging Research, Massachusetts General Hospital, Harvard Medical School, Charlestown, MA 02129, USA*

[b] *School of Computer Engineering, Inje University, Gim-Hae, Korea*

Abstract. *Aims*: To microscopically analyze the chemotherapeutic response of tumors using *in vivo* staining based on an annexinV-Cy5.5 probe and independently asses their apoptotic count using quantitative histological analysis. *Methods*: Lewis Lung Carcinomas cells, that are sensitive (CS-LLC) and resistant (CR-LLC) to chemotherapy were implanted in nude mice and grown to tumours. Mice were treated with cyclophosphamide and injected with a Cy5.5-annexinV fluorescent probe. *In vivo* imaging was performed using Fluorescence Molecular Tomography. Subsequently tumours were excised and prepared for histology. The histological tumour sections were stained for apoptosis using a terminal deoxynucleotidyl transferase-mediated nick end labeling (TUNEL) assay. A minimum of ten tissue sections were analyzed per tumour for apoptosis quantification by TUNEL staining and corresponding Cy5.5 distribution. *Results*: We detected higher levels of apoptosis and corresponding higher levels of Cy5.5 fluorescence in the CS-LLC vs. the CR-LLC tumours. The cell count rate on CS-LLC sections over CR-LLC was found to be $\sim 2:1$ where the corresponding area observed on Cy5.5 distribution measurements revealed a $\sim 1.7:1$ ratio of CS-LLC over CR-LLC. These observations are consistent with the higher apoptotic index expected from the CS-LLC cell line. *Conclusions*: Quantitative analysis of histological slices revealed higher fluorescence and higher apoptotic count in the CS-LLC tumour images compared to the CR-LLC tumour images. These observations demonstrate that the annexinV-Cy5.5 probe sensed the chemotherapeutic effect of cyclophospamide and further confirmed *in vivo* FMT measurements.

Keywords: Quantitative histological analysis, fluorescence molecular tomography, *in vivo* staining, TUNEL, apoptosis quantification, chemotherapeutic effect

1. Introduction

Non-invasive fluorescence imaging has emerged in recent years as an important *in vivo* method for small-animal research. This development has followed after the emergence of bio-compatible fluorochromes with molecular specificity that serve as reporter molecules *in vivo* in a variety of biotechnology applications [13, 14,27]. High-resolution imaging of histological slices using fluorescence microscopy and tissue sectioning with confocal and multi-photon microscopy typically use light in the visible spectral region. For probing deeper into tissues, fluorochromes that emit in the near infrared (NIR) are employed. Tissue penetration of several centimetres can be achieved in this spectral region, owing to low tissue absorption. Imaging in the NIR has spawned a new family of optical imaging techniques that are low resolution but that have significantly higher penetration depths than microscopy and retain high molecular specificity [11,18]. Optical imaging of small animals now incorporates several elegant technologies, including bioluminescence imaging [7,8], fluorescence planar (reflectance) imaging [2,3,20,26,28] and more recently tomographic imaging, in particular Fluorescence Molecular Tomography (FMT) that was developed to overcome limitations of planar imaging and improve on quantification and three-dimensional imaging. FMT has shown the abil-

*Corresponding author: Prof. Heung-Kook Choi, Obang-dong 607, School of Computer Engineering, Inje University, Gim-Hae, Gyung-Nam 621-749, Rep. of Korea. Tel.: +82 55 320 3437, C.P.: +82 10 6733 3437; Fax: +82 55 322 3107; E-mail: hkchoi@mitl.inje.ac.kr.

1570-5870/05/$17.00 © 2005 – IOS Press and the authors. All rights reserved

ity to image protease expression deep in tissues *in vivo* [15,16] and more recently it has recorded responses to anticancer treatment *in vivo* in small animals [17] using an annexin V-based reporter conjugated to the NIR fluorochrome Cy5.5 [18].

An important aspect in the development of new imaging methods is the establishment of appropriate standards to correlate the macroscopic appearance of fluorescent probes with the underlying biology. Importantly, in fluorescence imaging applications, the same fluorescent agent can be used for *in vivo* imaging and for histological staining. Therefore microscopic observations and macroscopic imaging can be referenced to each other to yield a more complete picture of fluorochrome bio-distribution. In contrast to planar imaging, FMT records fluorochrome bio-distribution volumetrically; i.e. it three-dimensionally resolves fluorochrome concentrations over regions of interest with millimeter to sub-millimeter resolutions [10]. For example, average fluorescence concentration values are reported for small sized tumours over the entire tumour volume. In-order to accurately correlate FMT findings with the underlying micro-distribution it is important to obtain multiple sections through the volume of interest and extract average fluorescence values. Besides using this approach for validating FMT observations with the underlying histology, average histological analysis can be used to summarize the histological appearance of different lesions for comparison purposes and yield concise descriptive measures of the underlying biology.

In this work, we quantitatively analyzed the micro-distribution of a Cy5.5-annexin V probe in Lewis Lung Carcinomas, treated with cyclophosphamide and observed histologically. We outline a methodology for obtaining average measures of the distribution of the injected probe and for correlation with the underlying apoptotic count [1,25]. Good agreement between these values and previously described macroscopic FMT measurements is obtained [17]. In the following, Section 2 describes the methods employed, Section 3 demonstrates key results of this analysis and Section 4 discusses the implications of the results and of obtaining co-registered macroscopic and microscopic observations.

2. Materials and methods

2.1. Cell culture and animal models

Cyclophosphamide-sensitive Lewis lung carcinoma (CS-LLC) cells and cyclophosphamide-resistant Lewis lung carcinoma (CR-LLC) cells were propagated in 10% foetal bovine serum and Dulbecco's modification of Eagle's medium. CS-LLC and CR-LLC cells were implanted in three female nu/nu mice as in [17]. One million (10^6) cells were injected subcutaneously and bilaterally in the upper anterior thorax of each mouse as shown in Fig. 1. Institutional approval was obtained for *in vivo* animal studies. Animals were imaged 9–12 days after implantation, when tumours were 4–5 mm in diameter. Cyclophosphamide (Mead Johnson, Princeton, NJ) was administered i.p. at 170 mg/kg. The first treatment was given at 72 h prior to imaging, and the second treatment was given at 24 h prior to imaging. Cy5.5-labeled annexin V (1 nmol/animal) prepared according to [18] was injected i.v. via the tail vein, at 2 h prior to imaging.

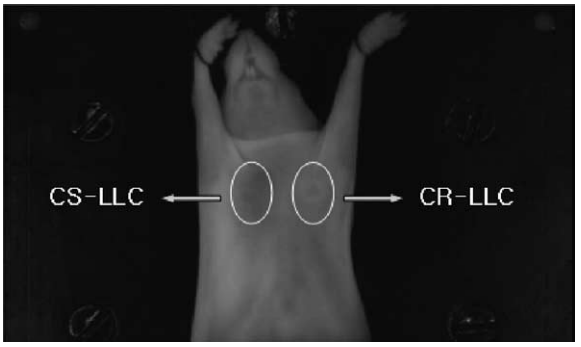

Fig. 1. The position of tumor implantation in the mouse.

2.2. Histological staining

Tumours excised from euthanized animals were snap frozen and cut into 10-μm sections. Approximately half of the sections were fixed in OCT for fluorescence microscopy and the remaining sections were stained for apoptosis using terminal deoxynucleotidyl transferase-mediated nick end labelling (TUNEL, ApopTag apoptosis detection kit, Serologicals Corporation, Norcross, GA) [6,24]. We followed the manufacturer's procedure for indirect staining of unfixed tissue cryosections and used secondary anti-digoxigenin F(ab′)2 mAb fragments (Roche Diagnostics Co, Indianapolis IN) conjugated to Cy3 dye (GE-Amersham). Stained sections were imaged using Zeiss Axiovert TV100 fluorescence microscope. A minimum of ten tissue sections per tumour were analysed for quantification of TUNEL-positive cells and cell-associated Cy5.5-annexin. The *in situ* staining of DNA strand breaks detected by the TUNEL assay and subsequent visualisation by light microscopy gives biologically

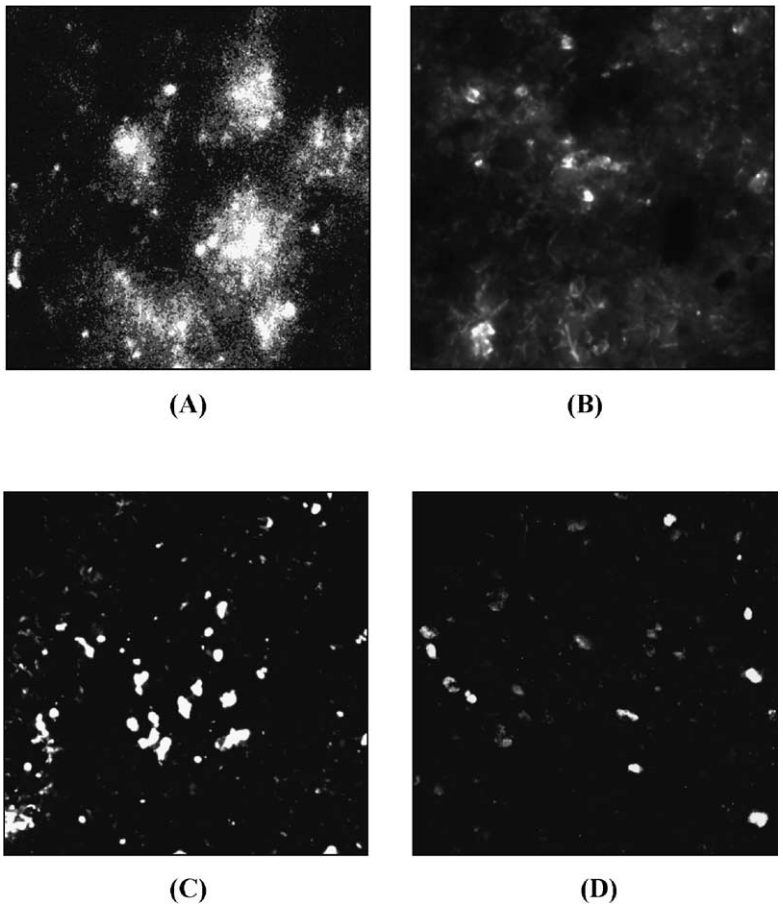

Fig. 2. Representative fluorescence microscopic images of M1, 512 × 512 pixels, 8 bits per pixel: (A) CS-LLC/Cy5.5, (B) CR-LLC/Cy5.5, (C) CS-LLC/Cy3 and (D) CR-LLC/Cy3.

significant data about apoptotic cells, which may be a small percentage of the total population [9,12]. Apoptotic cells stained positive with the ApopTag kit are easier to detect and more definitively identified than are cells in histochemically stained tissues.

2.3. Microscopic image acquisition

Fluorescence microscopy at 10× magnification was performed using an inverted microscope (Zeiss Axiovert 100 TV, Wetzlar, Germany) fitted with appropriate filter sets (Omega Optical, Brattleboro, VT), with spectral bands of 550–565 nm for Cy3 and 680–710 nm for Cy5.5. Images were acquired using a Photometrics CH250 CCD (Photometrics, Tucson, AZ), with image acquisition and storage controlled by IP LabSpectrum software (Signal Analytics, Vienna, VA). The camera resolution was 1035 × 1316 pixels at 12 bits per pixel. The total analysed histological images were 96 : 51 images of the CS-LLC and 45 images of the CR-LLC from three selected nude mice.

2.4. Image analysis

Image processing and analysis were performed using an image analysis tool (IMAN, MITL, Korea) which was programmed in Visual C++ running on a 2.2 GHz Pentium IV personal computer. For all histological slices, a central region of interest, 512 × 512 pixels, was selected to avoid inhomogeneous boundaries and ensure homogeneous illumination. Images were converted to 8 bits per pixel for improving computational efficiency. Figure 2 shows representative staining in each category.

Segmentation. The original microscopic images captured were subjected to histogram equalization to normalize all images to the same spread of intensities. Then, a threshold was applied to all images to con-

vert them to binary [4]. An advantage of using the histogram equalization was that one threshold value was employed for all volumes imaged as there was no need for a dynamic threshold to be applied. This process ensures that absolute image maxima, which varied significantly from study to study due to varying illumination strength and staining conditions, do not affect the calculation. The threshold used in this study was determined after histogram equalization based on a training set of images obtained from animal data-sets not included in this analysis, and it was fixed to a grey-level intensity value of 250 for Cy5.5 and Cy3 images.

Feature extraction. The quantification of the segmented objects involved implemented a labelling algorithm by selecting objects of more than 1 pixel size and using 8 neighbouring pixel clustering for counting object numbers [5,22]. Two main features were summarised, i.e. the number of objects and the total object area on an image. These factors were used to calculate quantitative average measures on histological appearance.

Statistical analysis. We employed a multivariate statistical analysis implemented in the SAS program package [21], in order to extract statistically significant changes of average area and object numbers calculated for CS-LLC vs. CR-LLC tumours for the Cy3 and the Cy5.5 images obtained. Both the variables and the histological samples were set as independent variables. The statistical significant differences were measured by means of the p-value, which was carried out using Student's t-test equality of variances between CS-LLC and CR-LLC measures. Moreover we calculated the maximum, minimum, and standard deviation in each category.

3. Results

Table 1 summarizes the results obtained from the Cy5.5 channel that map the distribution of the Cy5.5 annexin V probe. The results indicate significantly higher fluorescence both distribution and intensity from the CS-LLC compared to the CR-LLC as follows; On an average there were significantly higher number of objects observed (840 vs. 174) and higher total area observed (1.66 : 1) between the CS-LLC and CR-LLC respectively. Different tumours demonstrated different fluorescence distribution with higher CS-LLC to CR-LLC area ratios being that of mouse 3 at $\sim$2 : 1 and lower being that of mouse 1 at 1.32 : 1. In general we assumed that the fluorescence area better represents the fluorochrome concentration in the tumour as it reflects total Cy5.5 amount. These results were confirmed by macroscopic FMT observations recently published [17].

The results of the TUNEL staining are similarly summarised in Table 2. The CS-LLC tumour sections yielded on an average a significantly higher apoptotic cell count (2.09 : 1) compared to the CR-LLC sections. The total area measured however demonstrated only a slight area increase (1.06 : 1) indicating that generally smaller objects were observed on the CS-LLC sections. Sections obtained from the tumour of mouse one yielded a lower apoptotic count from the CS-LLC tumour compared to the CR-LLC.

The p-values for the mean number of objects found for mouse 1 (M1) CS-LLC vs. CR-LLC was $p < 0.0009$, for mouse 2 (M2) CS-LLC vs. CR-LLC it was $p < 0.0001$, and for mouse 3 (M3) CS-LLC vs. CR-LLC it was $p < 0.0001$ in the Cy5.5 channel and M1: $p < 0.4625$, M2: $p < 0.0001$, and M3: $p < 0.0001$ for the Cy3 channel. Respectively the p-values calculated for the mean area of objects found on the images were M1: $p < 0.0003$, M2: $p < 0.0001$, and M3: $p < 0.0001$ for the Cy5.5 channel and M1: $p < 0.0001$, M2: $p < 0.0081$, and M3: $p < 0.0011$ for Cy3.

In general, the cell count in the Cy3 slices appeared more variable on CS-LLC than on CR-LLC since there was greater heterogeneity between different sections in the Cy3 channel (apoptotic cells) compared to the corresponding analysis obtained in the Cy5.5 channel (Cy5.5-annexinV). Figure 3 summarizes the total number of pixels above the selected threshold value for each individual section slice analyzed. Generally the CS-LLC sections demonstrated higher variance of total number of pixels between slices compared to the CR-LLC.

4. Discussion

Small-animal optical imaging at the macroscopic level has been made possible by the development of planar and FMT imaging systems. As these techniques evolve, it is important to validate the macroscopic appearance of resolved fluorescent lesions with the underlying microscopic findings. The distributions of fluorochromes injected *in vivo* can be directly visualized by fluorescence microscopy after selecting the appropriate NIR wavelength. In parallel, immunohistochem-

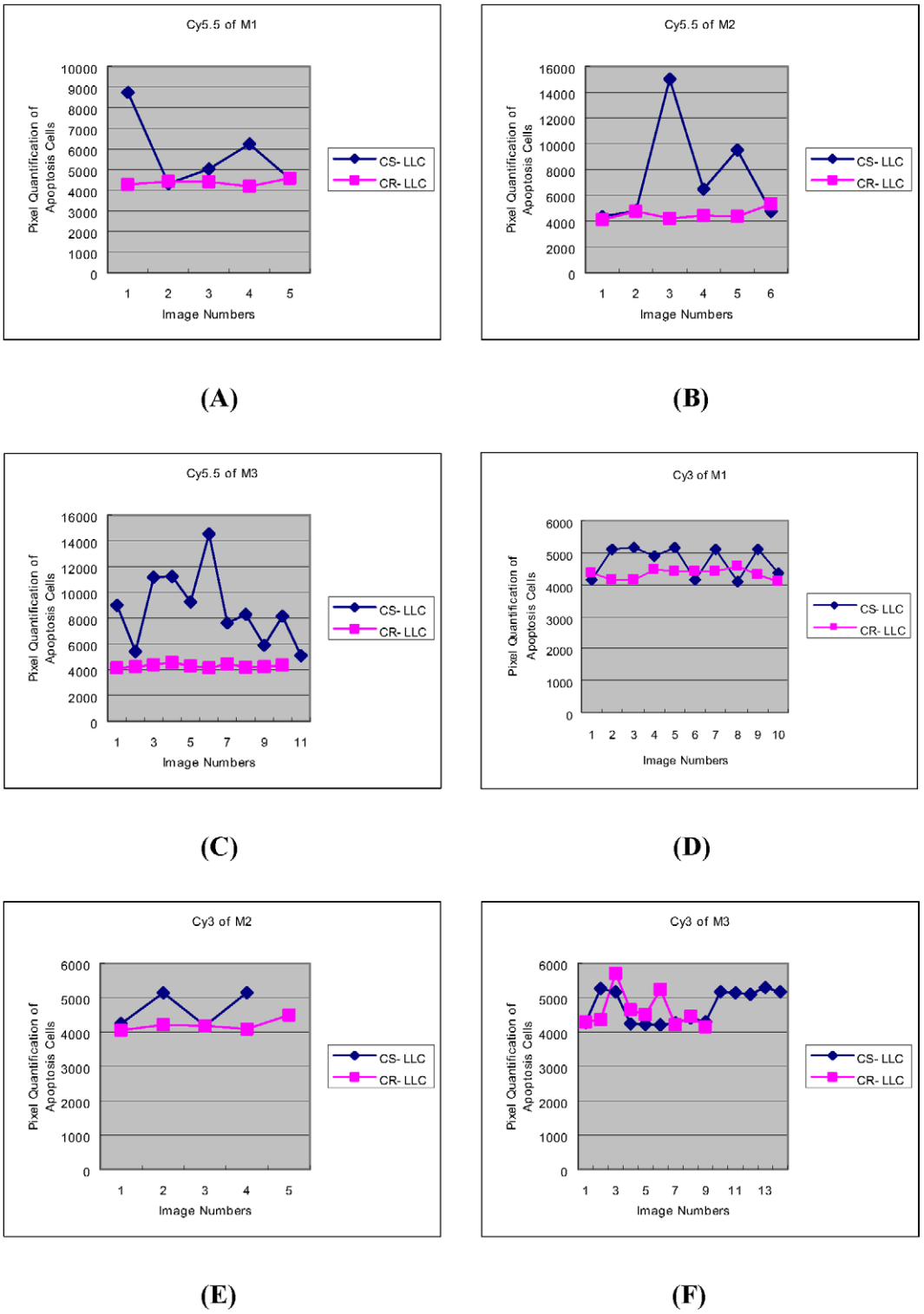

Fig. 3. Average histological appearance of the pixels above threshold, according to the methodology presented, for each section studied for CS-LLC (■) and CR-LLC (□) tumors. Appearance of (A) Cy5.5 of M1, (B) Cy5.5 of M2, (C) Cy5.5 of M3, (D) Cy3 of M1, (E) Cy3 of M2 and (F) Cy3 of M3 analysis.

Table 1
Quantification of the Cy5.5 annexin histological appearance in (a) CS-LLC and (b) CR-LLC tumors

Mouse	No. img.	Mean no. obj. (min, max)	St.d.	Mean area (min, max)	St.d.
		Carcinoma CS-LLC			
M1	5	191 (93, 387)	119	5775 (4320, 8740)	1816
M2	6	308 (71, 861)	300	7493 (4366, 15029)	4157
M3	11	341 (58, 986)	245	8701 (5093, 14548)	2839
Total	22	840 (222, 2234)	664	21,969 (13,779, 38,317)	8812
		Carcinoma CR-LLC			
M1	5	34 (19, 47)	13	4372 (4179, 4577)	150
M2	6	70 (44, 96)	26	4529 (4098, 5318)	448
M3	10	70 (33, 99)	24	4295 (4116, 4574)	146
Total	21	174 (96, 242)	63	13,196 (12,393, 14,469)	744

No. img.: number of images; Mean no. obj.: mean number of objects; Mean area: mean area of the quantification on an image.

Table 2
Quantification of TUNEL staining (Cy3 channel) for (a) CS-LLC and (b) CR-LLC tumors

Mouse	No. img.	Mean no. obj. (min, max)	St.d.	Mean area (min, max)	St.d.
		Carcinoma CS-LLC			
M1	10	91 (63, 169)	32	4719 (4100, 8328)	1319
M2	5	180 (36, 610)	242	4570 (4137, 6145)	882
M3	14	458 (69, 4679)	1215	4729 (4103, 11,259)	1881
Total	29	830 (168, 5458)	1489	14,018 (12,340, 25,732)	4082
		Carcinoma CR-LLC			
M1	10	132 (54, 186)	41	4325 (4097, 4557)	148
M2	5	67 (53, 84)	11	4202 (4052, 4491)	173
M3	9	97 (29, 246)	82	4615 (4153, 5705)	521
Total	24	397 (102, 479)	134	13,142 (12,429, 14,839)	819

ical studies may offer additional information on the presence of molecular targets or of the effect monitored and yield a more complete picture.

In this study we devised a methodology that analyzed the microscopic labelling of Lewis Lung Carcinomas using an annexinV-Cy5.5 fluorochrome and the correlative TUNEL staining to independently evaluate the apoptotic burden in treated tumours. In order to obtain average measures of the tumour appearance, we analyzed several sections obtained from the tumour volume and employed quantitative image analysis. Generally, the feature extraction of computer image analysis [19] may help solve the general problem of reproducibility. Tinacci et al. [23] compared cervicovaginal cytology slide sets with a digital set and evaluated inter-observer reproducibility after training. However, the standardisation of analyses with images captured in different environments is not simple. In the present study, there was significant intensity variation between slices obtained from different tumours or between the two wavelength channels. This is a typical behaviour, often the result of variation of microscope illumination strength, fluorochrome bleaching and other factors. The histogram equalisation and the thresholding method selected though appeared insensitive to these intensity fluctuations and resulted in a suitably robust and stable algorithm for analysis.

The histological appearance of the tumours yielded significantly higher fluorescence area indicating preferential accumulation in the CS-LLC tumour. This result confirms previous macroscopic observations using FMT [17]. Similarly, TUNEL staining yielded a significantly higher number of apoptotic cells. The overall area of the signals observed however was only slightly higher in CS-LLC vs. CR-LLC tumours. Generally the TUNEL staining appeared of higher variability in signal intensities observed between CS-LLC and CR-LLC. Characteristically in mouse 1 there was slightly less apoptotic count observed in the sensitive tumour vs. the resistant tumour. Interestingly, this tumour also

demonstrated small fluorescence differences between CS-LLC and CR-LLC even though the CS-LLC tumour demonstrated higher fluorescence than the CR-LLC. Such discrepancies may be a result of the selection of slices. Since different sections were used for the Cy3 and Cy5.5 analysis these results can reflect variability between slices. In addition there could biological differences between the bio-distribution of the annexin V probe and the underlying apoptosis, for example there may be some non-specific (not bound) bio-distribution of the probe in the tumours that could explain some differences that were seen on apoptotic count vs. Cy5.5 distribution.

Overall the proposed methodology can quantitatively link microscopic observations to macroscopic imaging using FMT or other methodologies. The relation with FMT however is of particular importance since it also provides for quantitative observations; qualitative histological observations would not suffice for accurate comparison between results. This combined macroscopic and microscopic quantification is potentially of great use in several basic research or clinical applications, especially when differences in biological effects and in different animals or tissue types need to be accurately observed.

Acknowledgements

The authors thank Dr. Timothy Browder (Children's Hospital, Harvard Medical School, Boston, MA) for the gift of the cyclophosphamide-resistant Lewis lung carcinoma variant. This research was supported in part by the National Institute of Health Grants No. RO1 EB 000750-2, R33 CA 91807. This research was supported by a research grant from the Korea Institute of Science & Technology Evaluation and Planning (KISTEP) under the Real Time Molecular Imaging Program.

References

[1] F.G. Blankenberg and H.W. Strauss, Noninvasive imaging using radioactive annexin V is an emerging strategy for the assessment of cell death in vivo, *Apoptosis* **6** (2001), 117–123.

[2] A. Bogdanov and R. Weissleder, The development of in vivo imaging systems to study gene expression, *Trends Biotechnol.* **16** (1998), 5–10.

[3] J.E. Bugaj, S. Achilefu, R.B. Dorshow and R. Rajagopalan, Novel fluorescent contrast agents for optical imaging of *in vivo* tumors based on a receptor-targeted dye-peptide conjugate platform, *J. Biomed. Opt.* **6** (2001), 122–133.

[4] H.K. Choi, J. Vasko, E. Bengtsson, T. Jarkrans, P.U. Malmstrom, K. Wester and C. Busch, Grading of transitional cell bladder carcinoma by texture analysis of histological sections, *Anal. Cell. Pathol.* **6** (1994), 327–343.

[5] H.K. Choi, T. Jarkrans, J. Vasko, E. Bengtsson, P.U. Malmstroem, K. Wester and C. Busch, Image analysis based grading of bladder carcinoma. Comparision of object, texture and graph based methods and their reproducibility, *Anal. Cell. Pathol.* **15** (1997), 1–18.

[6] D.R. Collingridge, M. Glaser, S. Osman, H. Barthel, O.C. Hutchinson, S.K. Luthra, F. Brady, L. Bouchier-Hayes, S.J. Martin, P. Workman, P. Price and E.O. Aboagye, In vitro selectivity, in vivo biodistribution and tumor uptake of annexin V radiolabelled with a positron emitting radioisotope, *Br. J. Cancer* **89** (2003), 1327–1333.

[7] C.H. Contag and M.H. Bachmann, Advances in in vivo bioluminescence imaging of gene expression, *Annu. Rev. Biomed. Eng.* **4** (2002), 235–260.

[8] T.C. Doyle, S.M. Burns and C.H. Contag, In vivo bioluminescence imaging for intergrated studies of infection, *Technoreview* **6** (2004), 303–317.

[9] Y. Gavrieli, Y. Sherman and S.A. Ben-Sasson, Identification of programmed cell death in situ via specific labeling of nuclear DNA fragmentation, *J. Cell. Biol.* **119** (1992), 493–501.

[10] E.E. Graves, J. Ripoll, R. Weissleder and V. Ntziachristos, A submillimeter resolution fluorescence molecular imaging system for small animal imaging, *Med. Phys.* **30** (2003), 901–911.

[11] H.R. Herschman, Molecular imaging: looking at problems, seeing solutions, *Science* **302** (2003), 605–608.

[12] J.F. Kerr, A.H. Wyllie and Currie, Apoptosis: a basic biological phenomenon with wide-ranging implications in tissue kinetics, *Br. J. Cancer* **26** (1972), 239–257.

[13] W.L. Monsky, D. Fukumura, T. Gohongi, M. Ancukiewcz, H.A. Weich, V.P. Torchilin, F. Yuan and R.K. Jain, Augmentation of transvascular transport of macromolecules and nanoparticles in tumors using vascular endothelial growth factor, *Cancer Res.* **59** (1999), 4129–4135.

[14] A. Nakayama, A.C. Bianco, C.Y. Zhang, B.B. Lowell and J.V. Frangioni, Quantitative of brown adipopse tissue perfusion in transgenic mice using near-infrared fluorescence imaging, *Mol. Imaging* **2** (2003), 37–49.

[15] V. Ntziachristos, A.G. Yodh, M. Schnall and B. Chance, Concurrent MRI and diffuse optical tomography of breast after indo-cyanine green enhancement, *Proc. Natl. Acad. Sci.* **97** (2000), 2767–2772.

[16] V. Ntziachristos, C.H. Tung, C. Bremer and R. Weissleder, Fluorescence molecular tomography resolves protease activity in vivo, *Nature Med.* **8** (2002), 757–761.

[17] V. Ntziachristos, E.A. Schellenberger, J. Ripoll, D. Yessayan, E. Graves, A. Bogdanov, Jr., L. Josephson and R. Weissleder, Visualization of antitumor treatment by means of fluorescence molecular tomography with an annexin V–Cy5.5 conjugate, *Proc. Natl. Acad. Sci.* **101** (2004), 12294–12299.

[18] A. Petrovsky, E. Schellenberger, L. Josephson, R. Weissleder and A. Bogdanov, Near-infrared fluorescent imaging of tumor apoptosis, *Cancer Res.* **63** (2003), 1936–1942.

[19] K. Rodenacker and E. Bengtsson, A feature set for cytometry on digitized microscopic images, *Anal. Cell. Oncol.* **25** (2003), 1–36.

[20] K. Singbartl, J. Thatte, M.L. Smith, K. Wethmar, K. Day and K. Ley, A CD2-green fluorescence protein-transgenic mouse reveals very late antigin-4-dependent CD 8^+ lymphocyte rolling in inflamed venules, *J. Immunol.* **166** (2001), 7520–7526.

[21] *Statistical Analysis System, 8.01*, SAS Institute Inc. Cary, NC, USA, 2001.

[22] J.R. Swedlow, I. Goldberg, E. Brauner and P.K. Sorger, Informatics and quantitative analysis in biological imaging, *Science* **300** (2003), 100–102.

[23] G. Tinacci, M.P. Cariaggi, F. Carozzi, A. Foggi, G. Miccinesi, F. Mirri, P. Pasquini, M. Zappa and M. Confortini, Digital images for interobserver variability comparison in cervicovaginal cytology, *Analyt. Quant. Cytol. Histol.* **25** (2003), 1–7.

[24] C. Van de Wiele, C. Lahorte, H. Vermeersch, D. Loose, K. Mervillie, N.D. Steinmetz, J.U. Vanderheyden, C.A. Cuvelier, G. Slegers and R.A. Dierck, Quantitative tumor apoptosis imaging using technetium-99m-HYNIC annexin V single photon emission computed tomography, *J. Clin. Oncol.* **21** (2003), 3483–3487.

[25] I. Vermes, C. Haanen, H. Steftens-Nakken and C. Reutelingsperger, A novel assay for apoptosis: Flow cytometric detection of phosphatidylserine expression on early apoptosis cells using fluorescein-labelled annexin V, *J. Immunol. Methods* **184** (1995), 39–51.

[26] R. Weissleder, C.H. Tung, U. Mohmood and A. Bogdanov, In vivo imaging of tumors with protease-activated near-infrared fluorescent probes, *Nature Biotechnol.* **17** (1999), 375–378.

[27] R. Weissleder, Scaling down imaging: molecular mapping of cancer in mice, *Nat. Rev. Cancer* **2** (2002), 1–8.

[28] M. Yang, L. Li, P. Jiang, A.R. Moossa, S. Penman and R.M. Hoffman, Dual-color fluorescence imaging distinguishes tumor cells from induced host agiogenic vessels and stromal cells, *Proc. Natl. Acad. Sci.* **100** (2003), 14259–14262.